TEC single wire resolution

– after calibration with the SMD –

Dimitri Bourilkov* **and Daniel Wagenaar†**

This note presents a study of the single wire resolution of the L3 TEC for data taken in 1994. For the main part of the detector the new SMD-based calibration gives a resolution which is 20 to 30% better than the one obtained with a TEC-based calibration. Inside the grid surrounding the anode the improvement is around a factor of two. The degradation of the resolution near the cathode is found to be much smaller than previously assumed. A significant asymmetry is observed between the two halves of each sector.

20 November 1995

* ETH, Zürich, e-mail: bourilko@cernvm.cern.ch
† Summer student at CERN from University of Amsterdam, e-mail: wagenaar@phys.uva.nl

1 Introduction

1.1 Calibration and resolution

The addition of a Silicon Micro-strip Detector (SMD) to the L3 experiment makes it possible to calibrate the Time Expansion Chamber (TEC) much more precisely and reliably than before [1]. Previously, the TEC was calibrated using mainly TEC information. This was an iterative and difficult procedure. The current calibration uses *mainly* outside information: SMD hits and transverse momentum from the μ-chambers. This method is non-iterative and much more stable.

Since the resolution of any detector depends strongly on the calibration, it is necessary to reassess the TEC resolution after each substantial change. Once the wire resolution is established, it is possible to improve the TEC fit by using for each hit an appropriate weight, depending not only on the drift length, but also on the individual half-wire and sector number. This will make the resolution on the fitted track parameters a bit better and, more important for some physics analyses, will give a reliable error matrix.

Our final goal is to establish a mechanism for synchronising the process of calibrating the TEC and determining its resolution. By storing the calibration and the resolution parameters in the same file which is written in the database, we can ensure that the average user will always get the latest TEC parameters, and most importantly, the right combination of them.

A similar study with less emphasis on the real data has been performed at the same time [2].

1.2 Definitions

A sketch of a part of the TEC, showing an inner sector and two outer sectors is presented in figure 1.

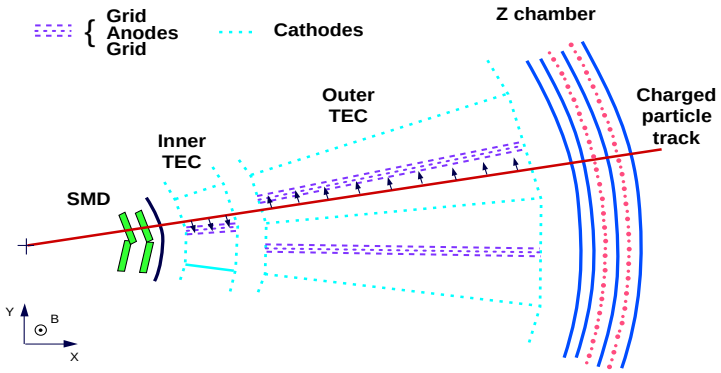

Figure 1: A sketch of a part of the TEC, showing an inner sector and two outer sectors. Also shown are the two layers of the SMD.

The half-sectors where electrons drift to the anode in the clockwise direction (i.e. from above in figure 1) are called positive half-sectors. Due to the Lorentz angle the drift will be slightly to the outside of the detector. Electrons that come from the other anode side, the negative half-sector, will drift slightly towards the inside of the detector.

For further details on the L3 TEC, see reference [3].

2 The method

2.1 Outline

We are both interested in global features of the resolution as a function of the position in the TEC, and in local (single half-wire) behaviour. Therefore we have set up a scheme that can improve an existing resolution function in either of two ways:

Iteration step 1: By mapping all sectors on top of each other (suitably scaled, see below), we can find global features, depending on wire number and drift distance (on either side of the wire).

Iteration step 2: By mapping the well-behaved part of the drift length for each half-wire onto one point (again using some scaling), we can study features of single half-wires.

If one would start with a resolution function that is completely ignorant of any feature of the TEC resolution (except perhaps for the general shape of the resolution as a function of drift distance), one would first perform iteration step 1, repeating it a number of times to let the output converge, and then perform iteration step 2. Since the results of both steps depend strongly on the input, it may be necessary to repeat them a few times to allow the system to settle down to the definitive resolution function.

2.2 Implementation

We collect a large number of tracks from $e^+e^- \longrightarrow \mu^+\mu^-$ and $e^+e^- \longrightarrow e^+e^-$ events, from the 94b run. We demand that a track consists of at least 40 hits. We impose no explicit cuts on the transverse momentum.

For each track we determine the unbiased residual at each hit, that is, we fit circular arcs through the data, each time excluding one particular hit. For this hit we then measure the signed distance between the hit and the fitted track[1]. Since this involves performing a large number of fits (equal to the number of tracks multiplied by the average number of hits on a track), an efficient fitting algorithm is a vital ingredient. We have used an adaptation of V. Karimäki's algorithm [4], which is particularly suited to fitting a lot of tracks through sets of almost the same data.

After fitting we perform the following procedure:

Let $R = R(w, s, d)$ be the old estimate of the TEC resolution as a function of *w*ire number, *s*ector number and *d*rift distance[2]. These variables are the most natural parametrisation of the (r, ϕ)-plane in the TEC. Setting (w_i, s_i, d_i, r_i) to the wire number, sector number, drift distance and residual found for each of the hits on all tracks, we may define the normalised residual:

$$\tilde{r_i} = \frac{r_i}{R(w_i, s_i, d_i)} \tag{1}$$

We can then compute the spread of the residuals in each individual (w, s, d)-bin. If $R(w_i, s_i, d_i)$ was already perfect, these spreads will all be equal to one. Because of this scaling, we may take a number of bins together, for example mapping all sectors on top of each other, and compute:

$$\tilde{\sigma}(w, d) \equiv \sigma(\{\tilde{r_i} | w_i = w \text{ and } d_i = d\}) \tag{2}$$

[1] Positive if the hit is farther from the anode than the fitted track, negative otherwise.

[2] The drift distance-axis differs from the perpendicular to the anode plane because of the Lorentz angle.

where $\sigma(A)$ denotes the standard deviation of a normally distributed set of data A.

We then obtain a better estimation R' of the resolution by setting:

$$R'(w,s,d) \equiv \tilde{\sigma}(w,d) \cdot R(w,s,d) \tag{3}$$

This summarises iteration step 1. Of course we could also compute:

$$\tilde{\sigma}(w,s) \equiv \sigma(\{\tilde{r_i} | w_i = w \text{ and } s_i = s\}) \tag{4}$$

and set:

$$R'(w,s,d) \equiv \tilde{\sigma}(w,s) \cdot R(w,s,d) \tag{5}$$

thus performing iteration step 2. Note that in equation (4) we only collect residuals from the part of the drift length where the field is homogeneous, which excludes the amplification region and the area near the cathodes.

2.3 Correcting for the accuracy of the fit

The method described in section 2.2 would work perfectly if the fitted tracks would exactly correspond to the true particle tracks. However, since the TEC has a finite resolution, this is not the case. The result is that there are two contributions to the residuals: one coming from the physical resolution of a hit, and one from the imperfection of the fit. We can write the relation between these quantities as:

$$\sigma_{res}^2 = \sigma_{hit}^2 + \sigma_{fit}^2 \tag{6}$$

where: σ_{res} denotes the spread of the residuals (at a certain point in the TEC),

σ_{hit} is the actual resolution of the hit (at that point),

σ_{fit} is the uncertainty in the position of the fitted track (at the location of the hit).

Near the centre of the tracks we would expect σ_{fit} to be approximately equal to σ_{hit} divided by the square root of the number of hits, increasing towards the ends as the lever arm increases.

Taking equation (6) into account, equation (2) should be changed into:

$$\tilde{\sigma}(w,d) \equiv \sqrt{\sigma^2(\{\tilde{r_i} | w_i = w \text{ and } d_i = d\}) - \tilde{\sigma}_{fit}^2(w,d)} \tag{7}$$

where $\tilde{\sigma}_{fit}(w,d) = \left\langle \frac{\sigma_{fit_i}}{R(w_i,s_i,d_i)} \right\rangle_{w_i=w;d_i=d}$. Equation (4) should be changed in the same way.

2.4 Producing a resolution function

Applying the method described above results in the resolution at each point in the TEC. However, the uncertainties are large. To produce a more accurate and manageable resolution function, we fit for each single half-wire the following function, with x the unsigned drift distance:

$$R(x) = \begin{cases} c_0 b_-(x) + f(x) b_+(x) & x < x_{grid} \\ f(x) & x_{grid} \leq x \leq x_{exp} \\ f(x) + g(x) & x > x_{exp} \end{cases} \tag{8}$$

where: $f(x) = c_1 + c_2 x + c_3 x^2$,

$g(x) = e^{c_4 + c_5 x}$,

$b_\pm$ is a connecting function: $b_\pm = \frac{1}{2} \pm \frac{1}{2} \tanh 4(x - 2.8)$,

c_i are fitting parameters,

x_{grid} is the grid distance: $x_{grid} = 3.2$ mm,

x_{exp} is the start of the area where the cathode wires cause serious inhomogeneities in the electric field: $x_{exp} = x_{cathode} - 5.2$ mm.

Note that the indices w and s have been suppressed in equation (8): c_0—c_3 are determined for each half-wire; c_4 and c_5 are determined for four groups of wires: positive and negative half-sectors separately for the inner and the outer TEC.

2.5 Numerical stability

2.5.1 Avoiding negative squares

Because of the minus sign in equation (7), care must be taken that $\sigma_{fit} \leq \sigma_{res}$. We would ordinarily expect σ_{fit} to be much less than σ_{res}, but statistical fluctuations may cause problems. This problem has been tackled using the following technique: we have not subtracted σ_{fit} from σ_{res} directly, but instead added σ_{fit} to $R(x)$ and fitted σ_{res} to the sum. (Note that 'sum', 'add', 'subtract' mean *quadratic* sum, addition, subtraction in this context.)

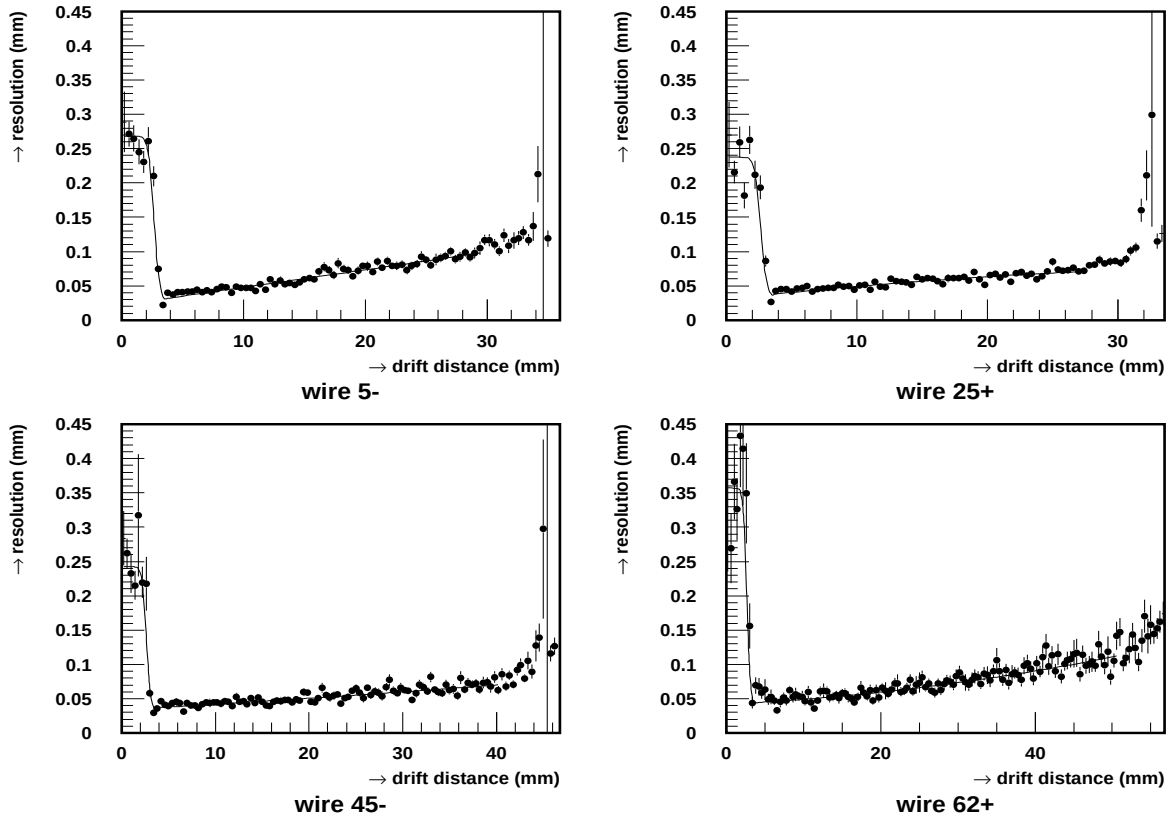

Figure 2: Results after performing iteration step 1 seven times: resolution versus drift distance for wires $5-$, $25+$, $45-$ and $62+$.

2.5.2 Empty bins

Another important problem is that of empty, or almost empty bins. This may happen accidentally in iteration step 1, if there is just not enough statistics, but more importantly, it may happen in iteration step 2 for wires that perform badly. A rather simplistic solution has been chosen for these problems: we just set σ_{res} to one if there are less than 100 entries in the histogram from which it would be determined for iteration step 1, and to zero for iteration step 2. Also σ_{fit} is set to zero if it cannot be determined properly. The errors on σ_{fit} and σ_{res} are set to large values, so that they will not affect the fitting for iteration step 1. For iteration step 2 on the other hand, this procedure will set the resolution function equal to zero independent of drift distance, clearly marking dead wires.

With the number of events we have used, there are normally some 600 hits per distance bin for iteration step 1, and some 1800 per half-wire for iteration step 2, so this method should indeed separate dead wires from working wires.

3 Results

We have started with a TEC resolution function, based on 1992 data and assuming no sector or wire number dependence, as implemented in subroutine TERESO of the official code (TEL3V192). Repeating iteration step 1 produced non-convergent results, the resolution function

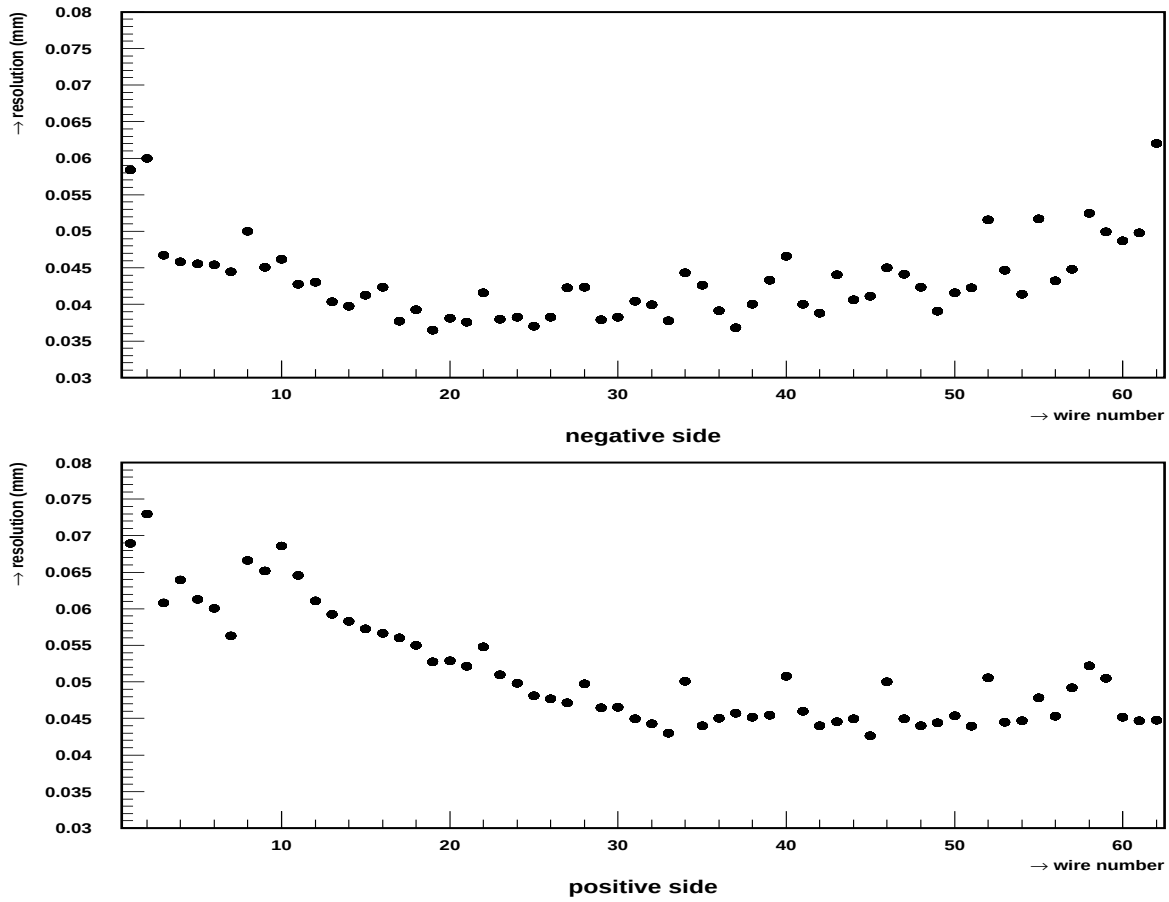

Figure 3: Resolution at 10 mm versus wire number, negative and positive sides, after seven iterations.

reaching clearly unphysical values around the seventh iteration. Therefore we have employed an initial resolution function produced as a by-product of the new calibration [1], which is based on tracks extrapolated from the SMD data using transverse momentum information from the μ-chambers. This function provides a starting point that is much closer to the actual TEC resolution, resulting in a stable iteration procedure.

Performing iteration step 1 seven times produced converging results. Figure 2 shows results for some typical wires. Note that at this stage iteration step 2 has not yet been performed, so all results are sector independent. Figure 3 shows the resolution at 10 mm from the anode, for all wires.

After these initial iterations, we performed iteration steps 2 and 1 repeatedly. Results after eight double iterations are shown in figures 4 and 5.

From figure 5 it can be seen clearly that there is a substantial asymmetry between positive and negative half-sectors: on the negative side, the resolution deteriorates at both ends of the detector, while on the positive side, the resolution only deteriorates at the inner end. The general shapes of the graphs are different. It can also be seen that the average resolution is slightly better for the negative half-sectors than for the positive half-sectors.

One feature that is present on both sides is the fact that wires 2, 8, 10 and then every sixth wire stick out from the rest. This feature can be seen even more clearly in figure 3. The cause of this difference is that these wires are charge division wires, which have special readout electronics to determine the z-coordinate of the hits on these wires. As a side effect, these electronics perform slightly worse in the (r, ϕ)-plane.

The most marked feature in figure 4 is negative half-sector four. Its resolution is far worse than that of the other sectors. This is caused by a known grounding problem in that sector. Half-

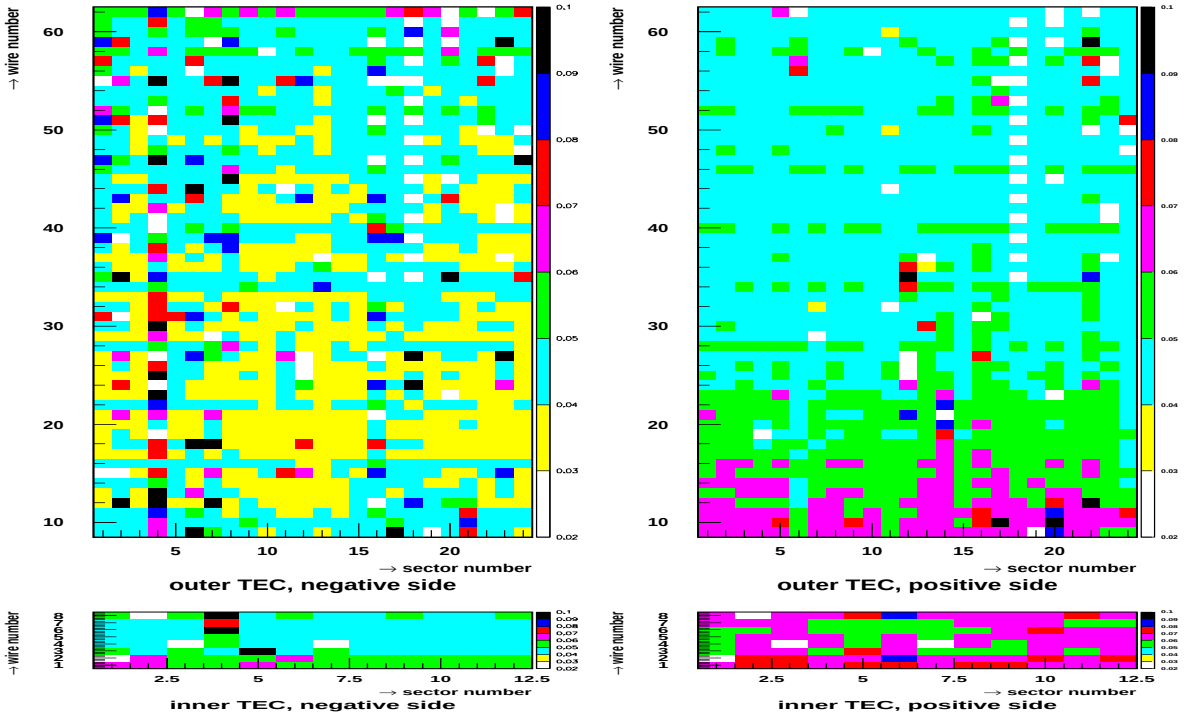

Figure 4: The resolution at 10 mm from the anodes for each half-wire. After another eight iterations, performing procedures 2 and 1 in turn, results for single half-wires have almost settled down. Scale is from 20 to 100 μm. Dead wires show up as white.

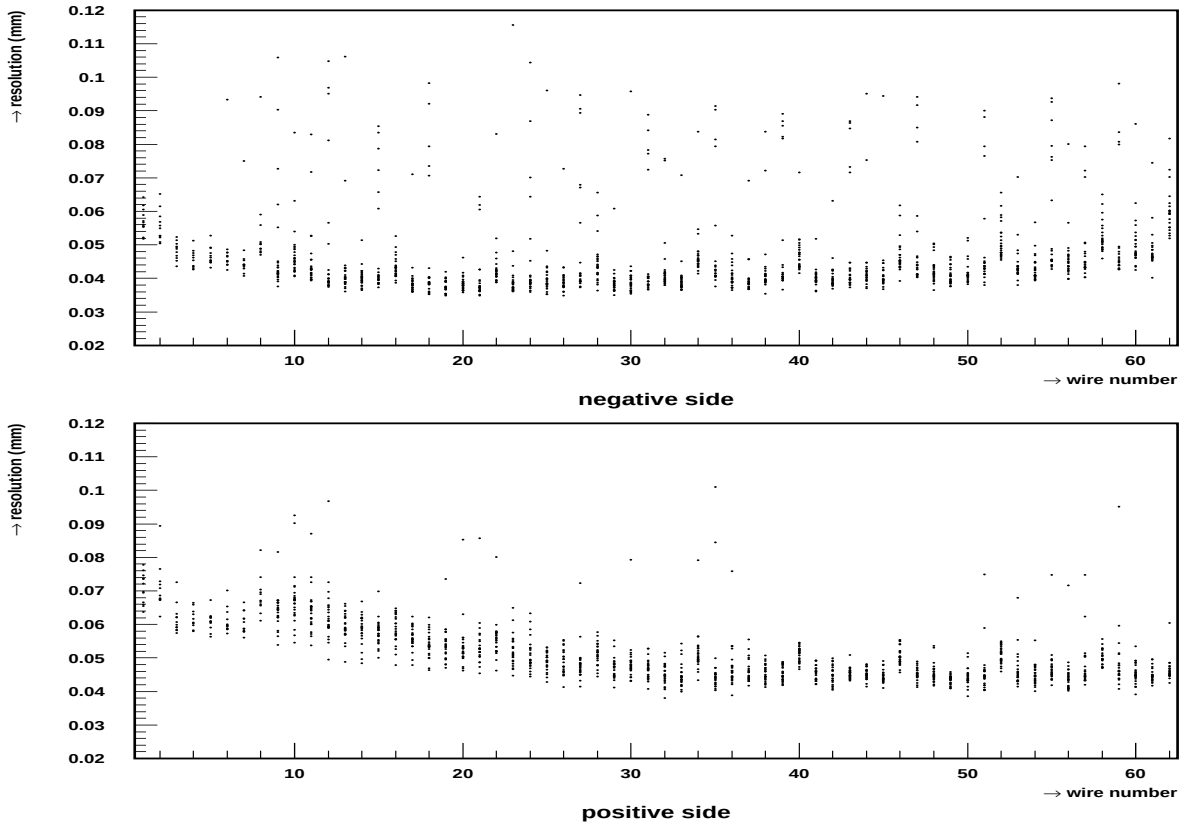

Figure 5: Showing the same data as figure 4, in a different way. Here the results for all sectors are plotted in the same column, making it impossible to see to which sector each point belongs. However, some general features are more clearly visible.

sector $16-$ is also worse than its neighbours, but less markedly so.

In figure 4 dead wires (wires which are not read out) are shown in white (as if their resolution were zero). Thus for example the known problem in sector 18 can be easily seen – from wire 35 onward every other wire is dead.

Figure 6 shows the resolution inside the grid in the same way figure 4 shows the resolution at 10 mm from the anode. Here no marked asymmetries occur, but the charge division wires are as clearly visible as outside the grid.

Finally, figure 7 shows the number of hits on each wire in the area selected for iteration step 2. The dead wires once more show up as white, and it can also be seen that sector $4-$ is behaving badly.

Another feature that shows up in these graphs is that for the sectors on the top and the bottom of the detector (around number 6 and number 18 in the outer TEC), the number of hits is slightly enhanced. This is probably caused by cosmics. Since these are also high energy tracks which pass close to the interaction point, it did not seem necessary to try to suppress them.

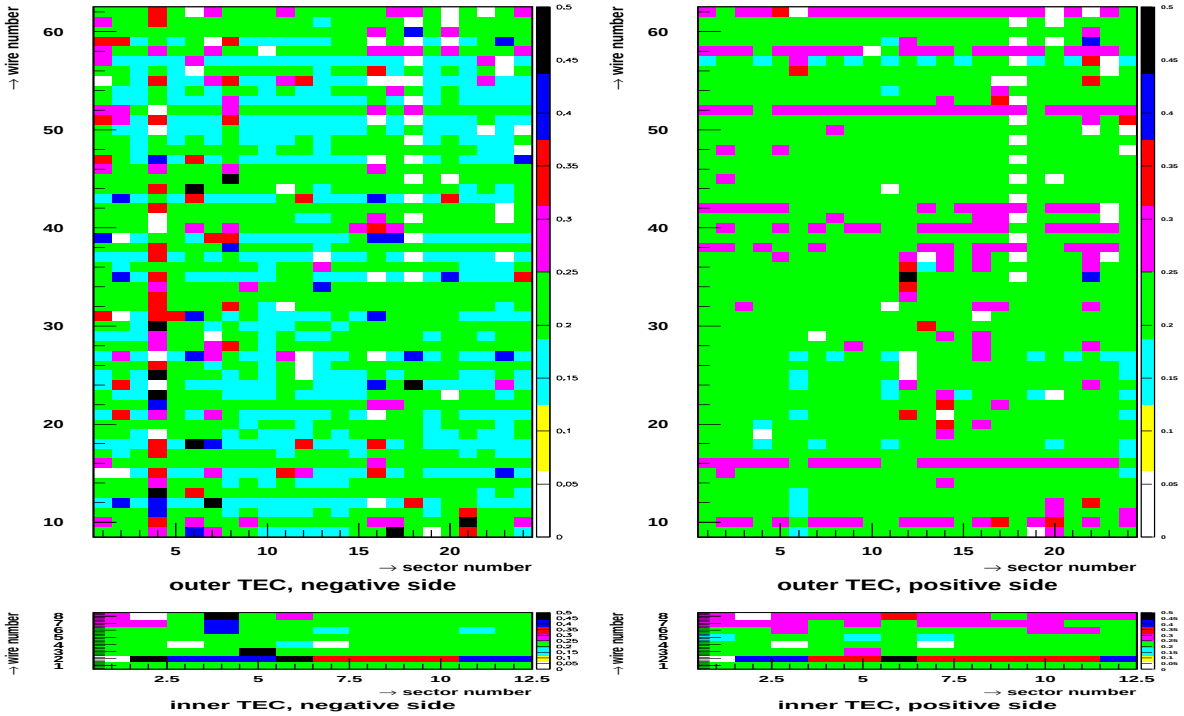

Figure 6: The resolution in the amplification area for each half-wire. Scale is from 0 to 500 μm.

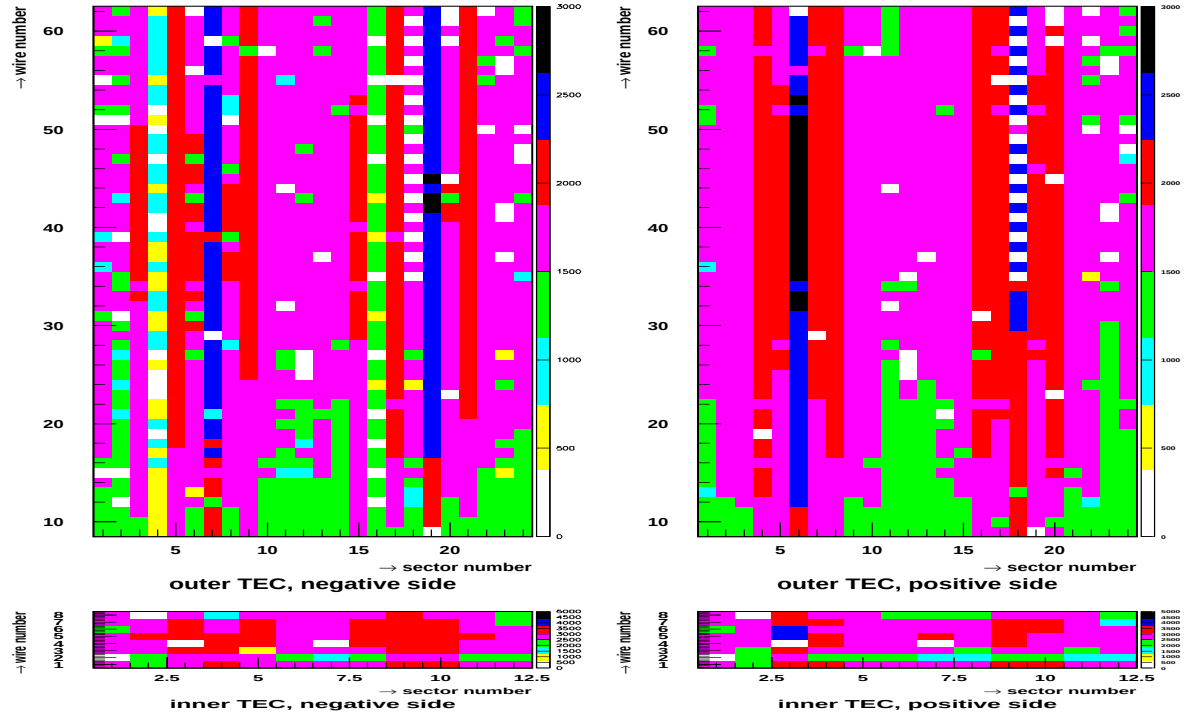

Figure 7: The number of hits on each half-wire as used for iteration step 2.

4 Discussion

4.1 Comparison with the 1992 resolution function

We compare the resolution function as found here with the one used in the tel3-code (V192). Figure 8 shows both the new and the old functions. The overall resolution is now much better than before. In the amplification area, the resolution is twice as good, and for larger drift distances the difference is also important: the degradation near the cathode is now confined to a much smaller area, and far less strong.

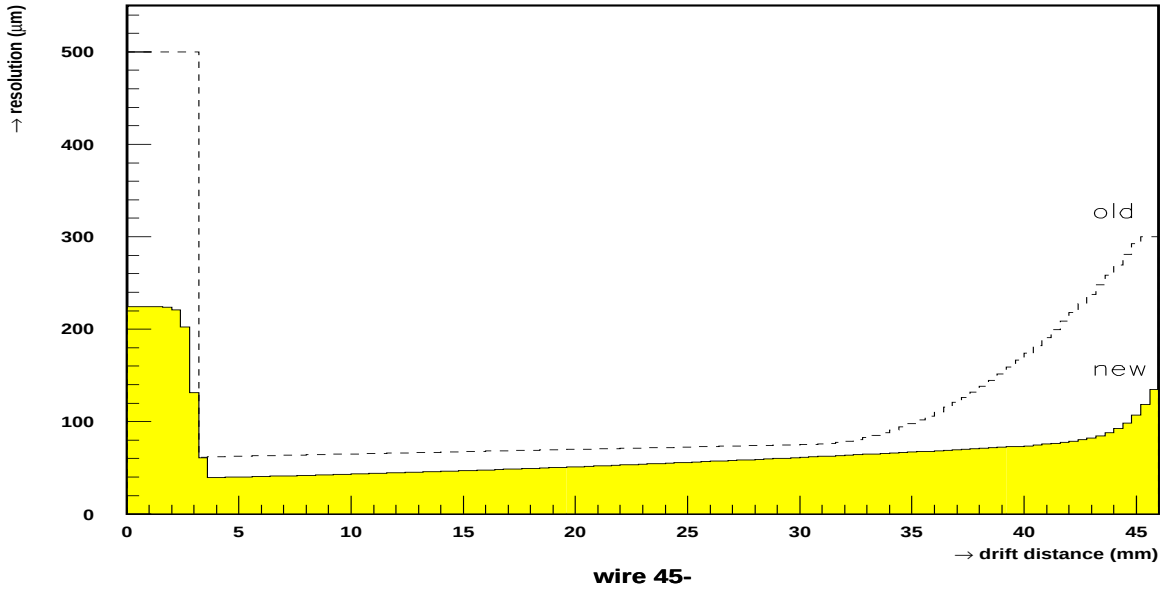

Figure 8: Comparison of old and new resolution functions for wire $45-$.

4.2 Wire dependence and asymmetry

Perhaps the most striking result of these studies is the qualitative asymmetry between positive and negative half-sectors, and the shapes of the plots in figures 3 and 5.

In order to understand these features we have re-examined the calibration procedure. The calibration parameters (e.g. the drift velocity) are obtained from fits to the Drift Distance to Time (DDT) relation, performed for each half-wire. In figure 9 we show the mean deviation of the TEC hits for a given half-wire from the fitted curve for the high-resolution part of the detector. All sectors are grouped together to enhance the wire dependence. We can observe that the quality of the fit is worse for the inner TEC (longer average drift distance!) and for the outermost wires of the outer TEC (ibid.). The deterioration as function of the wire number is more pronounced for the negative half-sectors. Most probably this reflects small inhomogeneities of the electric field leading to small perturbations (higher order terms).

The second quantity is the error in the hit position computed from the DDT relation [1], coming from the incertainty in the fitted calibration parameters (mainly C_1 and C_2 corresponding to the fitted effective grid position and the drift speed). The precision of these fits depends on the length of the lever arm available for a single wire, which is much shorter for the first part of the inner or outer TEC. So for the same (finite) number of tracks we should expect worsening of the resolution in these areas. We can expect to be free from this dependence only when we reach the

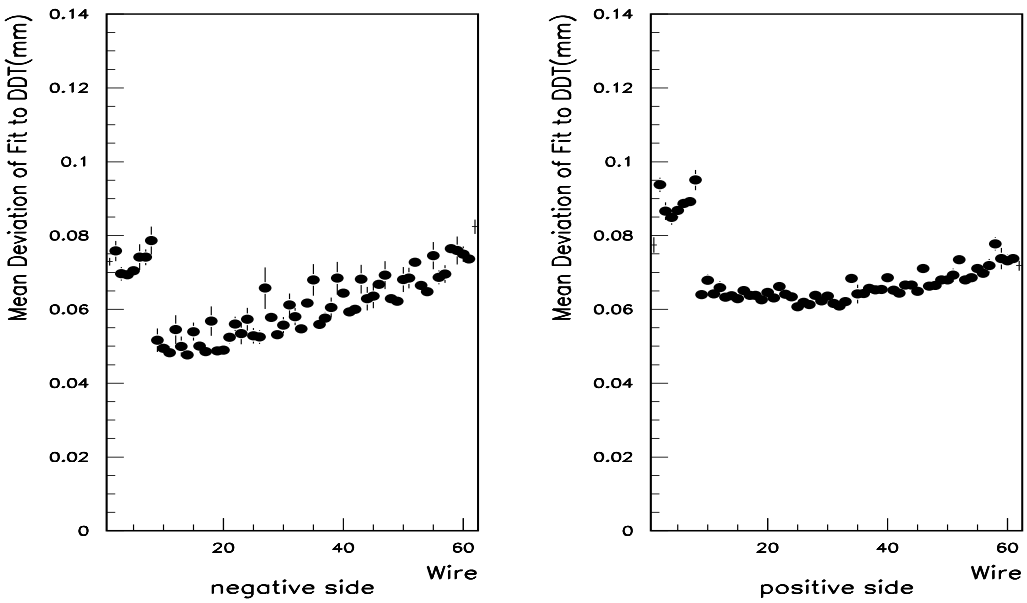

Figure 9: Mean deviation of the TEC hits from the fitted curve in the DDT fit as a function of wire number integrated over TEC sectors.

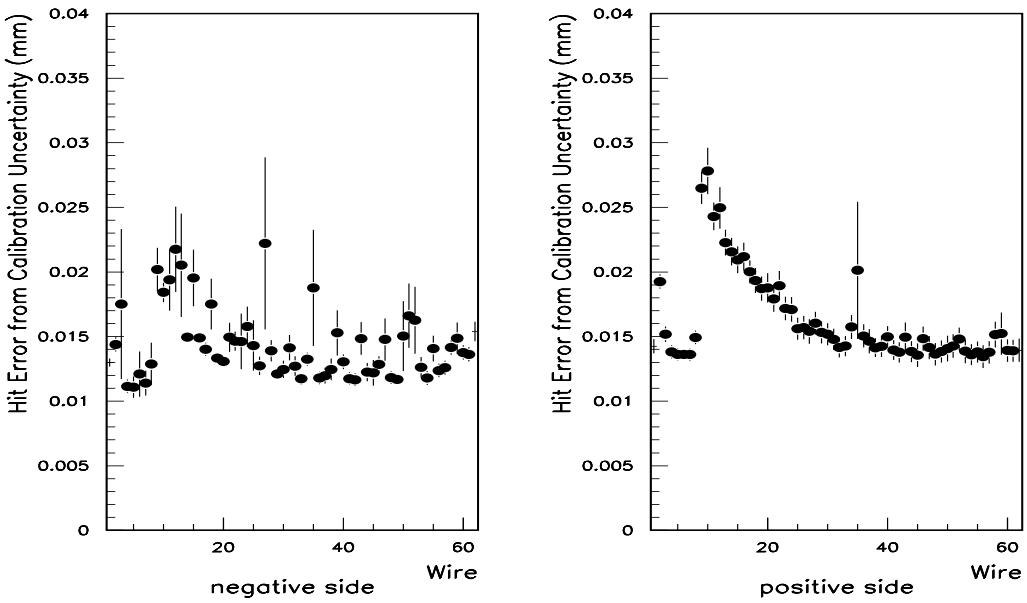

Figure 10: Hit error arising from the uncertainty on the fitted calibration parameters in the DDT fit at 20 mm from the anode as a function of wire number integrated over TEC sectors.

natural chamber limit. In figure 10 we show the hit error again as a function of the wire number. Clearly we are still limited by statistic. The effect is especially striking for the first wires of the outer TEC, where the drift distance is shortest. For the positive half-sectors the distance is shorter than for the negative half-sectors due to the Lorentz angle. This is probably an important contribution to the asymmetry in the hit errors which, as we have seen, is reflected also in the resolution functions.

4.3 The hobble in the centre of the inner sectors

A rather interesting feature of the σ_{res}-function for the inner wires is the small hobble than can be seen in the centre of the plot of wire $5-$. This hobble is even more pronounced for wires 1 and 8, as shown in figure 11.

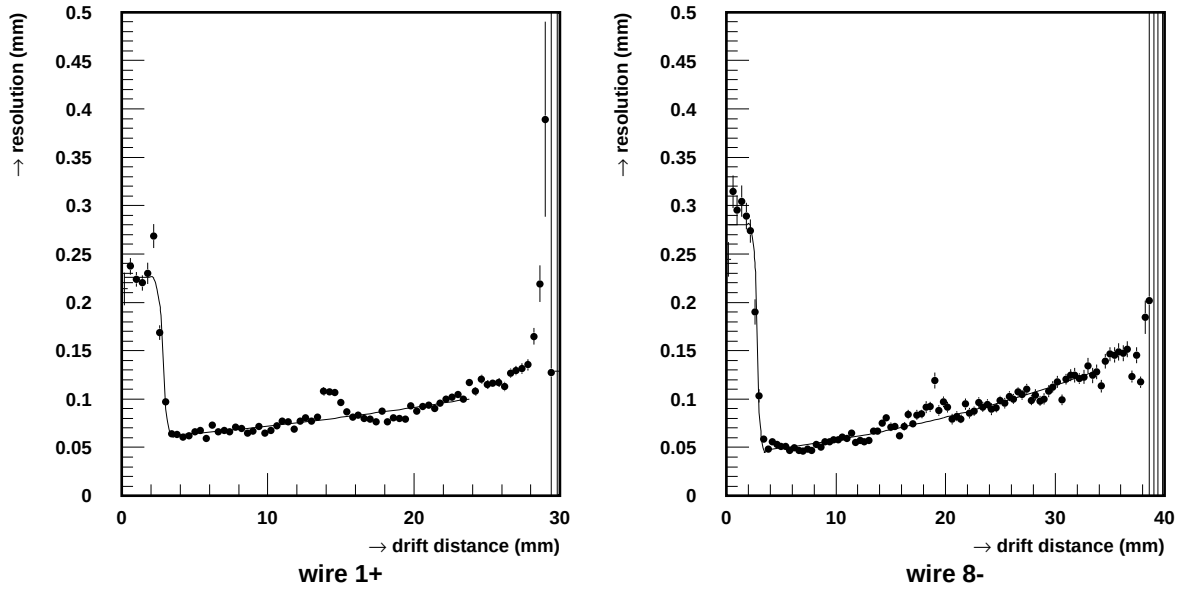

Figure 11: Hobbles in the resolution function for the inner wires.

The cause of these hobbles is the fact that tracks passing through the middle of an inner half-sector, will pass through the amplification area of an outer half-sector. Since the resolution there is far worse than in the drift region, this will lead to a highly increased σ_{fit}. However, as σ_{fit} is determined only globally for each half-wire, this hobble is not properly taken into account. Worse still, a major part of the increase in σ_{res} may be caused by incorrectly resolving the ambiguity in the position of the hits in the outer TEC: for hits very near the anode it is extremely difficult for the track reconstruction program to correctly determine whether the hit is in the positive or negative half-sector. The Monte Carlo system which is used to compute σ_{fit}, does not take this effect into account, so the hobble will be largely invisible on the σ_{fit} plots.

It is clear that these hobbles are not actually features of the resolution function of the inner wires. Therefore we have not tried to adapt $R(x)$ to include the effect. As killing the involved bins influenced the resolution function by a few percent only, which is less than the uncertainty of the fit, it was not considered necessary to take special measures to exclude the area containing the hobble at this stage. However, it should be a point of concern for future studies: it would be interesting to check if this effect could be reduced by killing some hits for which the ambiguity was not satisfactorily resolved.

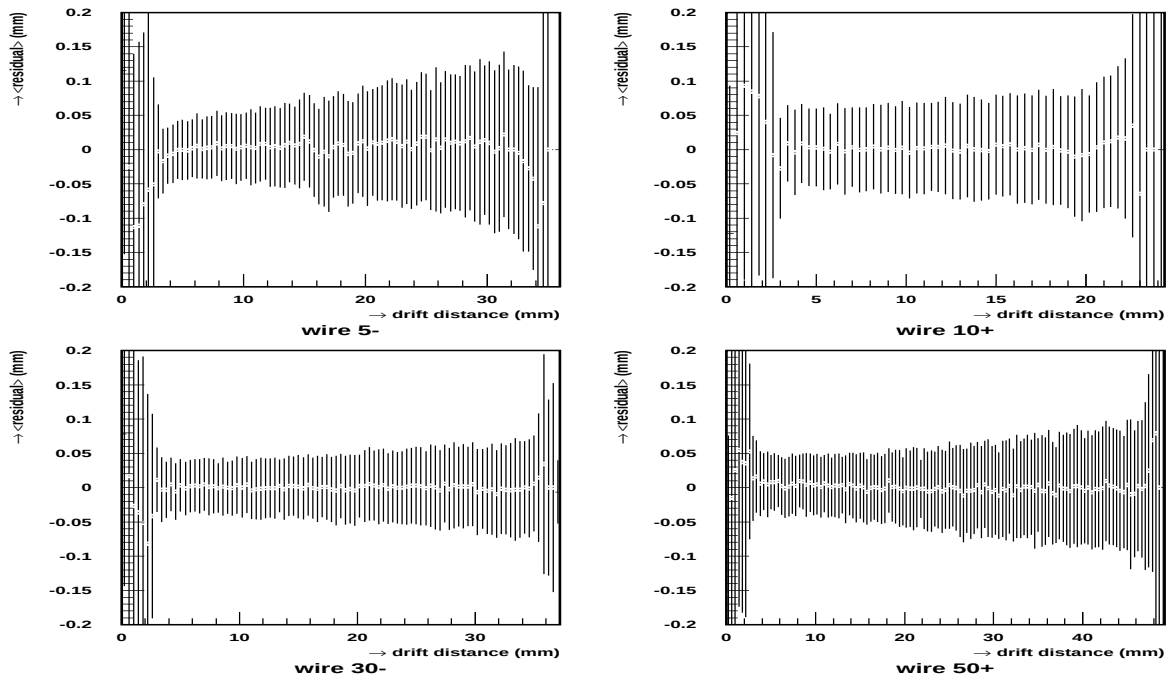

Figure 12: Average of the residuals versus drift distance for wires $5-$, $10+$, $30-$ and $50+$. The error bars indicate the spread, not the error on the average.

4.4 Test of the calibration

As a side effect these studies provide a test for the calibration: while computing the spread of the residuals at a certain point, the mean of the residuals is also found. For a small, but representative number of wires the results are shown in figure 12. In the major part of the drift length the chamber is well calibrated (the average of the residuals being less than 10% of the spread), but near the anode and the cathode the average tends to deviate from the zero line. The grid areas of some TEC sectors correspond to dead areas in the SMD, making a single wire calibration impossible. Therefore, only a global calibration, combining all TEC sectors for a given wire number, was performed in this region. In the cathode area we face two problems: low statistic for some wires and choice of the fitting function for the DDT relation. The third order polynomial used currently may not be sufficient to describe the highly non-linear behaviour very close to the field wires. In fact, until we find a way to improve the calibration in these delicate parts, the weight given to such hits should be substantially smaller than what is computed just from the spread, since the calibration uncertainty adds a non-negligible term.

5 Conclusions

The first conclusion from these studies is that the SMD-based calibration gives an important overall improvement for the TEC resolution, and especially in the amplification area and near the cathode wires.

The resolution parametrisation presented here describes the behaviour of the TEC in much more detail than previous ones. These details include:

- the global wire number dependence
- the asymmetry between negative and positive half-sectors

- the slightly worse resolution of the charge division wires, caused by differences in the read-out electronics
- the scaling of the resolution for each single half-wire.

The observed behaviour of the resolution functions is due partly to intrinsic features of the calibration procedure and possibly also due to characteristics of the chamber itself.

The resolution parameters are stored in the same file as the TEC calibration and the corresponding code to utilise them can be obtained from the authors.

The natural resolution limit, at least for some wires of the TEC, is still to be reached. So the logical follow-up for this work is a re-calibration based on the results presented here. A larger statistic could be obtained by using $e^+e^- \longrightarrow e^+e^-$ events in addition to $e^+e^- \longrightarrow \mu^+\mu^-$ events, as already done in the determination of the resolution function. Another important next step is to test these findings by checking if the Monte Carlo simulation matches the data when such a detailed resolution function is used.

6 Acknowledgements

We would like to thank G. Rahal-Callot, A.-P. Colijn, F. Linde and B. Zhou for valuable discussions. DW wishes to thank J. Engelen and J. Koch for helping him to get a summer student's position.

References

[1] D. Bourilkov: *TEC Calibration with the SMD*, L3 Note 1870, CERN, 1995.

[2] B. Zhou et al.: *Resolution Study on the L3 Time Expansion Chamber*, L3 Note 1835, CERN, 1995.

[3] F. Beissel et al.: *Performance of the L3 Central Tracking Chamber*, NIM, A332(1993)33.

[4] V. Karimäki: *Effective circle fitting for particle trajectories*, HU-SEFT-1990-04 / CERN UA1/TN/82-24, Helsinki 1990.